

# Fluorescence detection of phosphate in an aqueous environment by an aluminum-based metal-organic framework with amido functionalized ligands

Peng Li (✉)<sup>1,2</sup>, Lingqian Dong<sup>1,2</sup>, Han Jin<sup>3</sup>, Jingren Yang<sup>1</sup>, Yonghui Tu<sup>1</sup>, Chao Wang<sup>1,2</sup>, Yiliang He<sup>1,2</sup>

1 School of Environmental Science and Engineering, Shanghai Jiao Tong University, Shanghai 200240, China

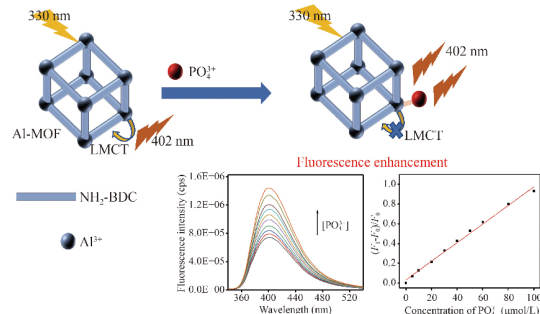
2 China-UK Low Carbon College, Shanghai Jiao Tong University, Shanghai 200240, China

3 Department of Instrument Science and Engineering, School of Electronic Information and Electrical Engineering, Shanghai Jiao Tong University, Shanghai 200240, China

## HIGHLIGHTS

- A novel Al-MOF was successfully synthesized by a facile solvothermal method.
- Al-MOF showed superior performance for phosphate detection.
- High selectivity and anti-interference for detection were demonstrated.
- The high coordination between Al-O and  $\text{PO}_4^{3-}$  was the key in fluorescence sensing.

## GRAPHIC ABSTRACT



## ARTICLE INFO

### Article history:

Received 13 December 2021

Revised 6 May 2022

Accepted 24 May 2022

Available online 15 July 2022

### Keywords:

Fluorescence  
Metal-organic framework  
Phosphate  
Detection  
Al-MOF

## ABSTRACT

The on-site monitoring of phosphate is important for environmental management. Conventional phosphate detection methods are not appropriate to on-site monitoring owing to the use of complicated detection procedures, and the consequent high cost and maintenance requirements of the detection apparatus. Here, a highly sensitive fluorescence-based method for phosphate detection with a wide detection range was developed based on a luminescent aluminum-based metal-organic framework (Al-MOF). The Al-MOF was prepared by introducing amine functional groups to conventional MIL to enhance phosphate binding, and exhibited excellent fluorescence properties that originated from the ligand-to-metal charge transfer (LMCT). The detection limit was as low as 3.25 μmol/L (0.10 mg/L) and the detection range was as wide as 3–350 μmol/L (0.10–10.85 mg/L). Moreover, Al-MOF displayed specific recognition toward phosphate over most anions and metal cations, even for a high concentration of the co-existent ions. The mechanism of phosphate detection was analyzed through the characterization of the combination of Al-MOF and phosphate, and the results indicated the high affinity between Al-O and phosphate inhibited that the LMCT process and recovered the intrinsic fluorescence of NH<sub>2</sub>-H<sub>2</sub>BDC. The recovery of the developed detection method reached a satisfactory range of 85.1%–111.0%, and the feasibility of on-site phosphate detection was verified using a prototype sensor for tap water and lake water samples. It was demonstrated that the prepared Al-MOF is highly promising for on-site detection of phosphate in an aqueous environment.

© Higher Education Press 2022

## 1 Introduction

In the present industrial society, phosphate-containing products have been extensively used, leading to the

inevitable release of a large quantity of phosphate into the aqueous environment. Unfortunately, excess phosphate (over 0.2 mg/L) can cause severe environmental effects such as eutrophication, excessive growth of algae, depletion of dissolved oxygen and death of aquatic organisms, leading to an imbalance in the aquatic ecology (Fan et al., 2020). Therefore, effective on-site monitoring

✉ Corresponding author

E-mail: lipeng2016@sjtu.edu.cn

through instantaneous detection of phosphate in aquatic environments is highly significant for the control and prevention of eutrophication. Furthermore, on-site detection of the molecule of interest is beneficial for obtaining a better understanding of its role in physicochemical processes (Wang et al., 2019). Currently, there are several well-developed methods for phosphate detection, including colorimetry, spectrophotometry, and chromatography (Li et al., 2010; Colina and Gardiner, 1999). However, these conventional detection methods are not suitable for on-site monitoring in the field, because they are time-consuming, generate waste liquid, and require professional operators and expensive apparatus. Some researchers developed electrochemical cobalt-based sensors for phosphate in order to reduce the cost and complexity of the instrumentation in field use, and obtained practical sensitivity with a detection limit of 3.16  $\mu\text{mol/L}$  (Zhu et al., 2014a). However, long-term stability is still a challenge for the cobalt-based sensors. Therefore, fluorescence-based approaches have attracted significant attention owing to their excellent properties of high sensitivity, rapid response, and ease of operation (Saini et al., 2016). Several luminescent probes have been reported for phosphate detection, mostly consisting of organic fluorescence dyes such as Rhodamine 6 G (Kröckel et al., 2014) and 2-pyridine-1H-imidazo[4,5-b]phenazine-zinc ensemble (Shi et al., 2014), and inorganic fluorescence nanomaterials including silver nanoclusters/metal–organic shell composite (Dai et al., 2015) and Mn-doped ZnTe/ZnSe quantum dots (Song et al., 2015). However, most of these probes exhibit shortcomings such as poor photostability and selectivity, and complicated preparation and sensing procedures.

Metal-organic frameworks (MOFs), consisting of metal ions/clusters and organic ligands, have attracted tremendous attention owing to their fascinating properties such as tunable crystalline structure, high porosity, large specific surface area and exposed active sites (Férey, 2008). These characteristics make them as attractive candidate materials or use in catalysis (Ma et al., 2009), gas storage (Zhang et al., 2013), drug delivery (Orellana-Tavra et al., 2016), and biological imaging (Horcajada et al., 2012). In particular, luminescent MOFs (LMOFs) have shown excellent performance in sensing detection, including metal cation (Wang et al., 2017), metal anion (Xu et al., 2018) and organics (Xie et al., 2018). The preferred analyte was easily bound to the probes due to their intrinsic porosity and functional groups. The selectivity and sensitivity of the detection method were improved through the pre-concentration of the guest molecules in the network (Yang et al., 2015). To date, several fluorescent probes based on LMOFs have been reported as sensing platforms for phosphate detection, including europium-based MOFs (Chandra Rao and Mandal, 2018; Chen et al., 2018; Zhang et al., 2019; Xu et al., 2015) and zirconium-based MOFs (Yang et al., 2015; Das et al., 2019; Gao et al., 2018). However, the practical application of the former is limited by the hazardous metal in waste liquid, whereas for the latter, the effective detection range achieved was not wide enough

to meet the requirement for monitoring the discharging source. According to the discharge standard for phosphate, the detection method should be effective in the range of 0.2–10 mg P/L (6.4–320  $\mu\text{mol/L}$ ). Hence, it is necessary to develop a novel fluorescent probe material with environmentally friendly constituent elements and a wide detection range.

The M-MIL (MIL=Materiaux de Institut Lavoiser) MOFs have recently attracted particular attention owing to their high chemical and thermal stability as well as water stability. Al-MIL MOFs are built from stable superter trahedral building units, containing unsaturated metal sites and accessible pores that are formed by rigid terephthalate ligands and trimeric octahedral clusters (Chen et al., 2005). Owing to its porous structure, Al-MIL was studied as a phosphate adsorbent (Liu et al., 2019). In addition to excellent absorptivity, it presented remarkable fluorescence characteristics. The high affinity of aluminum ion to inorganic phosphate makes Al-MIL promising candidates for specific recognition of phosphate via ligand exchange (Chen et al., 2018). Meanwhile, the introduction of amine functional groups to MOFs was confirmed to enhance phosphate binding by providing effective active sites that are more conducive to sensitive phosphate detection. It is important to note that according to our previous research, Al-MIL with different crystal structures were formed by the use of different solvents (Figs. S1 and S2), and their morphology, size (Fig. S3) and stability (Figs. S4 and S5) varied, which affecting the fluorescence characteristics of the interaction with phosphate (Fig. S6). The novel Al-MOF, synthesized with glacial acetic acid as the solvent, exhibits the best detection effect and can be applied to the fluorescence detection of phosphate.

This study seeks to develop a novel luminescent Al-based MOF by a facile one-pot solvothermal technique for use in the detection of phosphate in aqueous environments. The phosphate detection performance was evaluated in terms of selectivity, detection limit, and effective range. The mechanism of phosphate detection was analyzed through the characterization of the combination of Al-MOF and phosphate. The effectiveness of the on-site phosphate detection method was verified using a prototype sensor for testing the phosphate concentration of tap water and lake water.

## 2 Experimental

### 2.1 Chemicals and materials

All of the reagents used in this work were commercially available and of analytical grade and were used without further purification. Aluminum nitrate ( $\text{Al}(\text{NO}_3)_3 \cdot 9\text{H}_2\text{O}$ ) and N,N-dimethylformamide (DMF) were purchased from Sinopharm Chemical Reagent Co., Ltd. (China). 2-amino

terephthalic acid ( $\text{NH}_2\text{-H}_2\text{BDC}$ , 99%), glacial acetic acid,  $\text{KH}_2\text{PO}_4$ , and ethanol ( $\geq 99.7\%$ ) were obtained from Shanghai Titan Technology Co., Ltd. (Shanghai, China). Ultrapure water ( $18.2 \text{ M}\Omega \text{ cm}^{-1}$ ) was used as the solvent throughout the experiments. Solutions of various ions were prepared by dissolving the respective nitrate, sulfate, or chloride salts in deionized water.

## 2.2 Instruments and methods

All fluorescence spectra were measured using a FLS1000 fluorescence spectrometer (Edinburgh, UK) equipped with a 450 W xenon lamp. Powder X-ray diffraction (XRD) patterns were collected with a Shimadzu XRD-6100 diffractometer using  $\text{Cu K}\alpha$  radiation (Kratos, Japan). Fourier transform infrared (FT-IR) spectra were obtained using a Nicolet 6700 spectrometer (Thermo Fisher, USA) in the range of  $4000\text{--}400 \text{ cm}^{-1}$ . Scanning electron microscopy (SEM) images were observed by JEOL JSM-7800F Prime (ERSEM, JEOL, Japan). The transmission electron microscope (TEM) and elemental mapping images were obtained using a TALOS F200X instrument (FEI, USA). X-ray photoelectron spectroscopy (XPS) data were collected using an AXIS Ultra DLD instrument (Kratos, Japan). Thermogravimetric analysis (TGA) was carried out using a Pyris 1 thermogravimetric analyzer (Pekin Elmer, USA). Nitrogen adsorption–desorption isotherms were measured using an Autosorb-IQ3 analyzer (Quantachrome, USA). The specific surface area and micropore volume were calculated using the Brunauer–Emmett–Teller (BET) method. The zeta potential was measured using an Omni Nano C instrument (NanoBrook, Brookhaven, USA).

## 2.3 Preparation of Al-MOF

The Al-MOF was prepared by the solvothermal method according to previous work (Serra-Crespo et al., 2011) with slight modifications. Briefly,  $\text{Al}(\text{NO}_3)_3 \cdot 9\text{H}_2\text{O}$  (0.75 g, 2 mmol) and  $\text{NH}_2\text{-H}_2\text{BDC}$  (0.54 g, 3 mmol) were dispersed

into glacial acetic acid (30 mL) with the aid of ultrasonic treatment for 30 min, and then the mixture was sealed in a Teflon-lined reactor heated at  $150^\circ\text{C}$  for 48 h. After cooling to approximate  $20^\circ\text{C}$ , the yellow precipitate was centrifuged and washed with both DMF and ethanol three times and dried at  $50^\circ\text{C}$  for 12 h under vacuum to obtain the synthesized Al-MOF.

## 2.4 Phosphate anion sensing properties

The initial suspension of the fluorescent probe was prepared by dispersing Al-MOF powder samples (1.0 g) in ultrapure water (1000 mL) under ultrasonication for 10 min. Different probe concentrations were obtained by the dilution of the initial suspension solution. For aqueous phosphate sensing experiments, Al-MOF (5.4 mL) and phosphate (0.6 mL) were mixed in 10 mL centrifuge tubes. After incubating for 60 min at room temperature, the fluorescence spectra were collected.

## 2.5 Real sample detection by a fluorescence sensor

We also verified the performance of the on-site phosphate detection method and the fluorescence sensor using real environmental water samples. Tap water was collected from the campus of Shanghai Jiao Tong University. Lake water was collected from the Siyuan Lake of Shanghai Jiao Tong University. These samples were filtered with  $0.45 \mu\text{m}$  membranes to remove impurities. Then, the water samples were pretreated using a Ba-type ion chromatography column to remove  $\text{SO}_4^{2-}$  and  $\text{SO}_3^{2-}$ , and the pH of the water samples was adjusted to 4.2 in order to eliminate the influence of  $\text{CO}_3^{2-}$  and  $\text{HCO}_3^-$  (Fig. S7).

## 3 Results and discussion

### 3.1 Characterization of Al-MOF

The powder XRD pattern (Fig. 1a) of Al-MOF matched well with the simulated pattern derived from the single

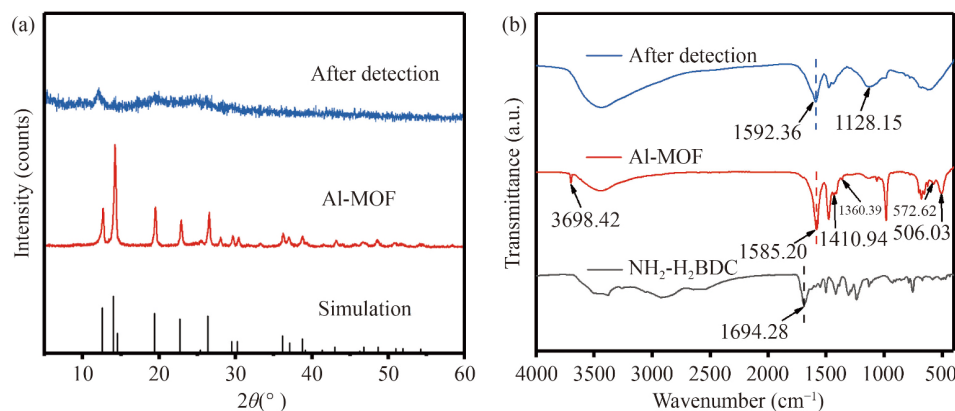


**Fig. 1** (a) XRD patterns of Al-MOF and Al-MOF after  $\text{PO}_4^{3-}$  detection; (b) comparison of the FT-IR spectra of  $\text{NH}_2\text{-H}_2\text{BDC}$ , Al-MOF, and Al-MOF after  $\text{PO}_4^{3-}$  detection.

crystal X-ray diffraction data, indicating the successful synthesis and high phase purity of Al-MOF. The FT-IR spectra of the free ligand and Al-MOF are shown in Fig. 1b. The stretching vibration of C = O ( $1694.28\text{ cm}^{-1}$ ) in the ligand shifted to  $1585.20\text{ cm}^{-1}$  in the Al-MOF, indicating the complete deprotonation of carboxylic groups (Cheng et al., 2018). The characteristic Al-O ( $572.62\text{ cm}^{-1}$ ) and Al-O-C ( $506.03\text{ cm}^{-1}$ ) peaks revealed that  $\text{Al}^{3+}$  ions successfully coordinated with carboxylic groups (Serra-Crespo et al., 2011). The peak at  $3698.42\text{ cm}^{-1}$  for Al-MOF can be assigned to Al-OH groups, formed by the  $\text{Al}^{3+}$  ions coordinated with dissociated water molecules, indicating the presence of abundant binding sites acting as recognition centers toward the P-O bonds of phosphate (Li et al., 2018). The SEM images (Figs. 2a and 2b) demonstrated that Al-MOF crystals had almost regular hexagonal shapes with sizes in the approximate range of 0.2–0.8  $\mu\text{m}$ . The appearance of the Al element in the TEM mapping images (Fig. 2f) and the Al 2p peak in the XPS analysis (Fig. 3a) revealed the successful coordination of  $\text{Al}^{3+}$  in Al-MOF. The  $\text{N}_2$  adsorption-desorption isotherms of Al-MOF (Fig. S8) presented type IV isotherms and implied the mesoporous structure of the material. The BET specific surface area and pore volume of Al-MOF were calculated to be  $102.93\text{ m}^2/\text{g}$  and  $19.1\text{ nm}$ , respectively. TGA (Fig. S9) revealed that Al-MOF had a good thermal stability and was stable up to  $300\text{ }^\circ\text{C}$  under air atmosphere.

### 3.2 Luminescence properties of Al-MOF

To understand the interaction between Al-O and the  $\text{NH}_2\text{-H}_2\text{BDC}$  organic ligand in the Al-MOF, luminescence

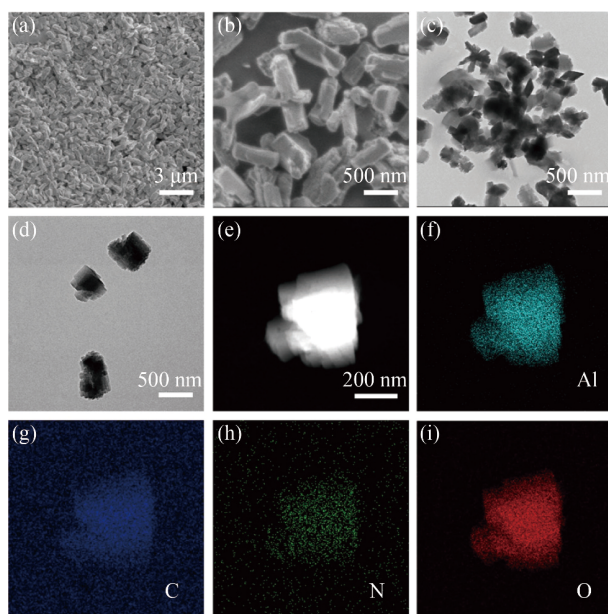


**Fig. 2** (a) and (b) SEM image of Al-MOF; (c)–(e) TEM images of Al-MOF; (f)–(i) element mapping of Al, C, N, and O, respectively.

studies on both the free  $\text{NH}_2\text{-H}_2\text{BDC}$  ligand and Al-MOF in the solid state and in aqueous solutions were performed at room temperature. As shown in Fig. S9a, the  $\text{NH}_2\text{-H}_2\text{BDC}$  ligand exhibited two weak fluorescence emission peaks at  $487\text{ nm}$  and  $571\text{ nm}$  that are ascribed to the  $\pi \rightarrow \pi^*$  electronic transition of the aromatic ring (He et al., 2014). The blue-shift of the emission wavelength of Al-MOF compared to  $\text{NH}_2\text{-H}_2\text{BDC}$  arises from the ligand-to-metal charge transfer (LMCT) (Yang et al., 2013). More interestingly, Al-MOF exhibited a rather weak fluorescence emission peak at  $402\text{ nm}$ , compared with the luminescence emission peak at  $456\text{ nm}$  of  $\text{NH}_2\text{-H}_2\text{BDC}$  (Fig. S10b). Except for the above LMCT effect, this phenomenon can be explained based on from the effect of solvent-induced fluorescence quenching. As reported in previous work, when water molecules enter the cavities, the electron transfer from the ligand to metal is affected via weak hydrogen bonds by coupling with Al-O clusters (Lu et al., 2011). Furthermore, the luminescence intensity of Al-MOF at the emission wavelength of  $402\text{ nm}$  was clearly enhanced upon the introduction of phosphate. These characteristic luminescence properties suggested that Al-MOF is highly promising as a fluorescent probe for phosphate detection in an aqueous environment.

### 3.3 Fluorescence sensing of phosphate

To obtain improved detection accuracy for phosphate detection, detection conditions, namely the fluorescent probe concentration, incubation time, and solution pH were optimized. The fluorescence emission spectra (Fig. S11) of Al-MOF showed that  $\lambda_{\text{ex}} = 330\text{ nm}$ ,  $\lambda_{\text{em}} = 402\text{ nm}$  can be used as suitable detection conditions. As illustrated in Fig. S12, with the increasing concentration of Al-MOF, the fluorescence intensity of the probe increased remarkably and then reached a plateau at approximately  $300\text{ mg/L}$ . The subsequent decline in the fluorescence intensity may be due to the reduction of fluorescence transmittance in the solvent. Furthermore, the examination of the four curves in Fig. S13 indicated that probe concentration affects the detection range of  $\text{PO}_4^{3-}$ . The curves corresponding to low probe concentrations ( $10$  and  $50\text{ mg/L}$ ) were more consistent with the pseudo-second-order kinetic model. The initial rapid fluorescence enhancement efficiency can be attributed to the abundant binding sites. After a period of time, the lower concentration of available sites and blocked cavities decreased the adsorption rate and the fluorescence enhancement efficiency. Based on this phenomenon, the probe concentrations of  $20$ ,  $100$  and  $200\text{ mg/L}$  were used for phosphate detection. In addition, considering the concentration range of phosphate tested in real water samples, the concentration of  $20\text{ mg/L}$  was selected for the subsequent experiments. The stability of Al-MOF refers to the stability of the fluorescence intensity during the detection process, which is the basis of the fluorescence detection method and without which the

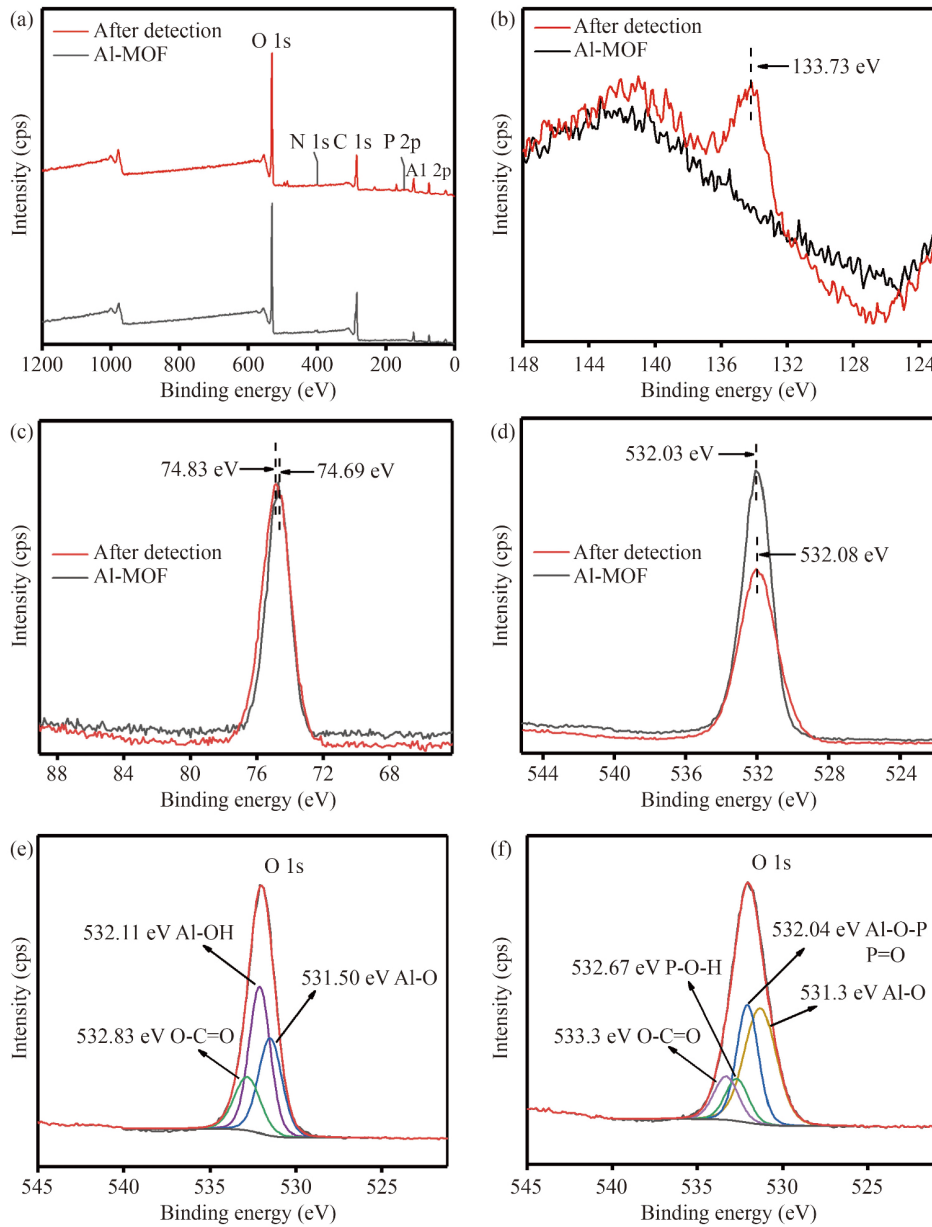


**Fig. 3** (a) Full range XPS spectra of Al-MOF and Al-MOF after  $\text{PO}_4^{3-}$  detection; (b) XPS spectra of P 2p; (c) XPS spectra of Al 2p; (d) XPS spectra of Q1s; (e) the magnified O 1s XPS spectra of Al-MOF; (f) the magnified O 1s XPS spectra of Al-MOF after  $\text{PO}_4^{3-}$  detection.

accurate detection cannot be achieved. Therefore, the influence of the incubation time on fluorescence sensing was also investigated (Fig. S14). Considering the detection time and fluorescence equilibrium, 60 min was selected as the reaction time for the subsequent experiments. As illustrated in Fig. S15, the characteristic fluorescence peak ( $\lambda_{\text{ex}} = 330 \text{ nm}$ ,  $\lambda_{\text{em}} = 402 \text{ nm}$ ) of Al-MOF clearly showed desirable fluorescence stability in solution with a wide pH range from 4 to 10 compared with the pH range of 6–9 in the actual water quality monitoring. Such behavior most likely arises from the electrostatic interaction between the positively charged  $-\text{NH}_3^+$  formed from the  $-\text{NH}_2$  on the surface of Al-MOF accepting the hydrogen

protons and the phosphate anions. For all subsequent experimental solutions, the pH range was 4.5–6.5, so that the pH of the solution does not affect the experimental results.

Under the optimized experimental conditions, fluorescence emission spectra of Al-MOF (20, 100, and 200 mg/L) for different concentrations of introduced phosphate were obtained at room temperature. As illustrated in Figs. 4a, 4c, and 4e, the fluorescence intensity at 402 nm gradually increased with the  $\text{PO}_4^{3-}$  concentration in the ranges of 0–20, 0–100, and 0–350  $\mu\text{mol/L}$ , respectively. Meanwhile, the fluorescence enhancement efficiency showed a good linear correlation with the  $\text{PO}_4^{3-}$  concentration in the

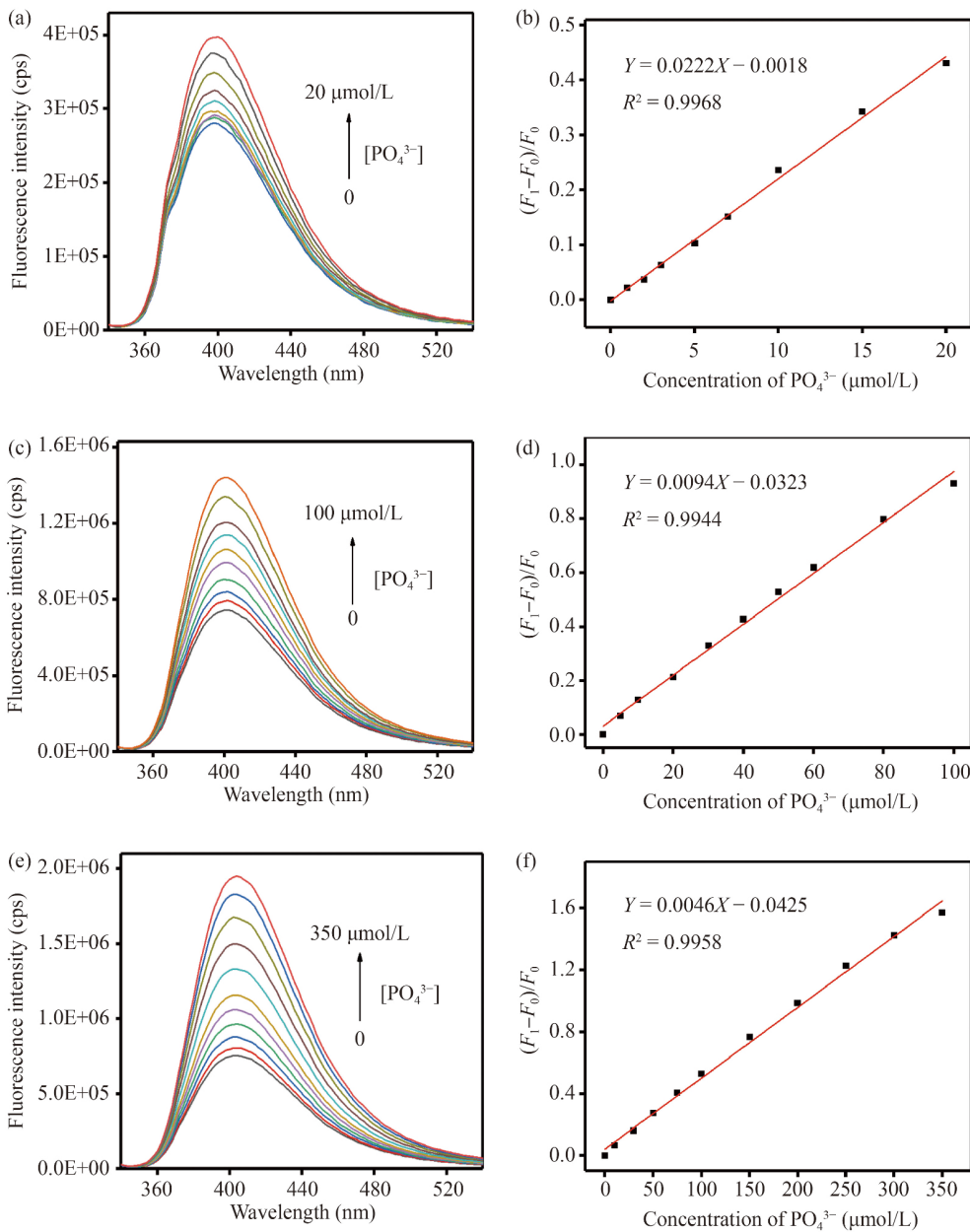


**Fig. 4** (a), (c) and (e) Fluorescence emission spectra of Al-MOF with the concentrations of 20, 100, and 200 mg/L in the presence of different concentrations of PO<sub>4</sub><sup>3-</sup> under  $\lambda_{\text{ex}}=330$  nm at room temperature. (b), (d) and (f) Linear plots of the fluorescence enhancement efficiency of Al-MOF with the concentrations of 20, 100, and 200 mg/L as a function of PO<sub>4</sub><sup>3-</sup> concentration.

ranges of 1–20 (Fig. 4b), 5–100 (Fig. 4d), and 10–350 μmol/L (Fig. 4f), respectively. The three calibration functions can be described as  $(F_1-F_0)/F_0 = -0.0018 + 0.0222C$  (20 mg/L),  $(F_1-F_0)/F_0 = 0.0323 + 0.0094C$  (100 mg/L) and  $(F_1-F_0)/F_0 = 0.0425 + 0.0046C$  (200 mg/L), where C is the PO<sub>4</sub><sup>3-</sup> concentration (μmol/L), and F<sub>1</sub> and F<sub>0</sub> are the fluorescence emission intensities of Al-MOF in the presence and in the absence of PO<sub>4</sub><sup>3-</sup>, respectively. Moreover, the calibration curves showed high correlation coefficients ( $R_1^2 = 0.9968$ ,  $R_2^2 = 0.9944$ ,  $R_3^2 = 0.9958$ ), and the limit of detection (LOD) was calculated as  $3\sigma/m$  (Das and Biswas, 2017). The LOD of Al-MOF with 20 mg/L

for phosphate is 0.10 mg/L (3.25 μmol/L), much lower than the 0.5 mg/L value that is the standard for phosphate discharge to aqueous environment. Hence, the detection sensitivity met the detection requirement of phosphate discharge. The detection range depends on the inherent properties of Al-MOF rather than on the co-existing matter. This method for phosphate detection with three concentrations of Al-MOF possessed a low detection limit and a wide detection range from 3 to 350 μmol/L; these results are quite competitive with those of other fluorescence detection methods reported in the literature, as summarized in Table 1.

**Table 1** Comparison of the phosphate detection capabilities of Al-MOF and other fluorescent materials

Materials	Detection limit ( $\mu\text{mol/L}$ )	Detection range ( $\mu\text{mol/L}$ )	References
Eu-BTB	10	10–100	Xu et al., 2015
{[EuL(H <sub>2</sub> O) <sub>1.35</sub> (DMF) <sub>0.65</sub> ]·1.9DMF} <sub>n</sub>	0.052	0.1–15	Cheng et al., 2018
{Eu <sub>2</sub> L <sub>3</sub> (DMF)}·2DMF	6.62	3–30	Chandra Rao and Mandal, 2018
Eu@BUC-14	0.88	5–150	Zhang et al., 2019
UiO-66-NH <sub>2</sub>	1.25	5–150	Yang et al., 2015
Zr-UiO-66-N <sub>2</sub> H <sub>3</sub>	0.196	0.025–0.25	Das et al., 2019
RhB@UiO-66-NH <sub>2</sub>	2	80–400	Gao et al., 2018
ZnO QDs + MOFs	0.053	0.5–12	Zhao et al., 2014
Al-MOF	3.25	3–350	This work

### 3.4 Selectivity and interference sensing of phosphate

High selectivity and anti-interference capacity are critical for fluorescence probe detection of phosphate. Hence, the fluorescence responses of Al-MOF were studied in the presence of various anions including F<sup>-</sup>, Cl<sup>-</sup>, Br<sup>-</sup>, CO<sub>3</sub><sup>2-</sup>, HCO<sub>3</sub><sup>-</sup>, NO<sub>3</sub><sup>-</sup>, NO<sub>2</sub><sup>-</sup>, SO<sub>4</sub><sup>2-</sup>, SO<sub>3</sub><sup>2-</sup>, and metal cations such as K<sup>+</sup>, Na<sup>+</sup>, Ca<sup>2+</sup>, Mg<sup>2+</sup>, Cu<sup>2+</sup>, Zn<sup>2+</sup>, Fe<sup>2+</sup>, Fe<sup>3+</sup>, and Al<sup>3+</sup>. As expected, Figs. 5a and 6a show that only phosphate resulted in a drastic fluorescence enhancement effect, whereas no obvious fluorescence changes were observed from other ions, demonstrating the high selectivity of Al-MOF toward phosphate. Then, interference experiments with coexisting substances were also conducted. It was noted that the concentration of anions used in the anti-interference experiments in the previously reported studies did not reach the levels in real aqueous

environments; thus, the reported probe performance results are also dubious (Yang et al., 2015; Cheng et al., 2018; Zhang et al., 2019). Our results (Figs. 5b and 6b) demonstrated that the CO<sub>3</sub><sup>2-</sup> and HCO<sub>3</sub><sup>-</sup> anions exhibited significant attenuation effects at 1 mM, whereas HCO<sub>3</sub><sup>-</sup> at 10 mmol/L and SO<sub>4</sub><sup>2-</sup>, and SO<sub>3</sub><sup>2-</sup> at 1 mmol/L and 10 mmol/L, respectively, exhibited remarkable enhancement effects. No significant fluorescence changes were observed for other ions, even when the concentration of the interfering ions was at least fifty times higher than that of phosphate, confirming the good anti-interference ability of Al-MOF with respect to co-existent anions. Then, for the detection of phosphate in real water samples, the water samples were passed through a Ba-type ion chromatography pretreatment column in order to remove SO<sub>4</sub><sup>2-</sup> and SO<sub>3</sub><sup>2-</sup> anions, and the pH of the solution was adjusted to 4.2 to eliminate the influence of the CO<sub>3</sub><sup>2-</sup> and HCO<sub>3</sub><sup>-</sup> anions.

Natural organic matters (NOM) in aqueous environments have significant fluorescence properties. According to the published reports, the peak of Al-MOF, which is at 330 nm/408 nm ( $E_x/E_m$ ), is not coincident with the peak for the NOM (Chen et al., 2003). Moreover, compared to the fluorescence intensity of Al-MOF, the fluorescence intensity of NOM is weak, and its influence can be ignored.

### 3.5 Mechanism of phosphate detection

To gain an in-depth understanding of the mechanism of the phosphate detection by Al-MOF, zeta potential measurements, FT-IR spectroscopy, and XPS spectra were used. In the presence of phosphate, the interactions between Al-MOF and phosphate leads to the collapse of Al-MOF and the formation of irregularly shaped complexes (Fig. S16). Correspondingly, the specific surface area and

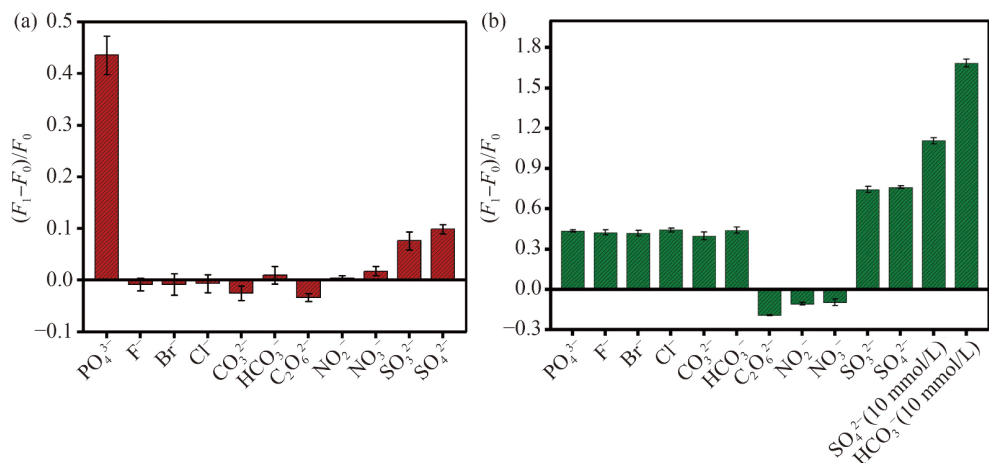


**Fig. 5** (a) Comparison of the fluorescence of the Al-MOF (20 mg/L) in the presence of different anions (20  $\mu\text{mol/L}$ ); (b) effects of different coexistent anions (1 mmol/L; for SO<sub>4</sub><sup>2-</sup> and HCO<sub>3</sub><sup>-</sup>, the concentration is 10 mmol/L) on the fluorescence response of Al-MOF (20 mg/L) upon the addition of 20  $\mu\text{mol/L}$  PO<sub>4</sub><sup>3-</sup>.  $F_0$  and  $F_1$  indicate the fluorescence intensity of Al-MOF without and with anions, respectively ( $\lambda_{\text{ex}}=330 \text{ nm}$ ,  $\lambda_{\text{em}}=402 \text{ nm}$ ).

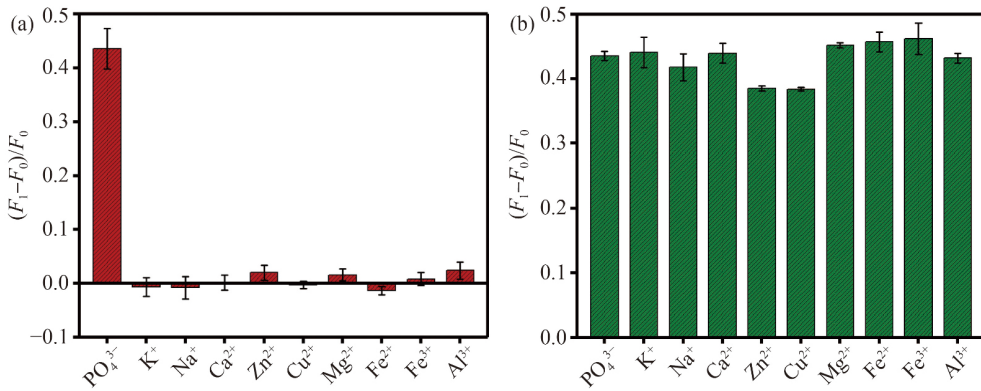


**Fig. 6** (a) Comparison of the fluorescence response of the Al-MOF (20 mg/L) towards different metal ions (20  $\mu\text{mol/L}$ ); (b) effects of different coexistent metal ions (1 mmol/L) on the fluorescence response of Al-MOF (20 mg/L) upon the addition of 20  $\mu\text{mol/L}$   $\text{PO}_4^{3-}$ .  $F_0$  and  $F_1$  indicate the fluorescence intensity of Al-MOF without and with anions, respectively ( $\lambda_{\text{ex}}=330 \text{ nm}$ ,  $\lambda_{\text{em}}=402 \text{ nm}$ ).

pore size changed to  $231.29 \text{ m}^2/\text{g}$  and  $3.06 \text{ nm}$  (Fig. S17), respectively. These observations were also consistent with the XRD analysis in Fig. 1a, indicating the sensitivity of Al-MOF to phosphate. The zeta potentials of the Al-MOF in the absence and presence of phosphate were measured to be  $+33.15 \text{ mV}$  and  $+24.4 \text{ mV}$  (Fig. S18), respectively, revealing the existence of electrostatic interactions between Al-MOF and phosphate. Additionally, FT-IR spectra of Al-MOF were measured in the absence and presence of phosphate (Fig. 1b). After incubation with phosphate, the broad P-O stretching vibration bands between  $900$  and  $1200 \text{ cm}^{-1}$  centered at  $1128.15 \text{ cm}^{-1}$  (Sun et al., 2015) confirmed the inclusion of phosphate into the framework of Al-MOF. Meanwhile, the disappearance of the Al-OH groups at  $3698.42 \text{ cm}^{-1}$  present in the pristine sample indicated that phosphate was absorbed by binding with the Al-OH groups on the surface of Al-MOF. In addition, the C=O stretching vibration of the carboxylic group in the phosphate-incubated Al-MOF exhibited a blue-shift to  $1592.36 \text{ cm}^{-1}$  from  $1585.20 \text{ cm}^{-1}$  of the pristine Al-MOF. This shift demonstrated the coordination effect between the Al-O clusters and phosphate, that weakens the interactions between the  $\text{NH}_2\text{-H}_2\text{BDC}$  ligands and Al-O clusters, leading to greater freedom and stronger vibrations of carboxylic groups (Zhu et al., 2014b). Further elucidation was performed based on the XPS spectra. As shown in Fig. 3, the appearance of the P 2p peak (Fig. 3b) and the shift of the Al 2p spectra (Fig. 3c) at  $74.83 \text{ eV}$  slightly toward higher binding energies indicated possible electron transfer in the valence band of Al 2p and the formation of Al-O-P (Liu et al., 2019). This may be due to the combination of the  $\text{Al}^{3+}$  ions with the more electronegative P-O bonds leading, to the loss of electron density and increased binding energy (Cheng et al., 2018). The deconvolution of the O 1s spectrum (Fig. 3f) in Al-MOF after  $\text{PO}_4^{3-}$  detection reveals four peaks that were assigned to O in Al-O (531.3 eV), Al-O-P and P=O (532.04 eV), P-O-H (532.67 eV), and O-C=O (533.3 eV).

Based on the above results, the mechanism of phosphate detection by Al-MOF can be reasonably suggested to be as follows. The fluorescence of the  $\text{NH}_2\text{-H}_2\text{BDC}$  organic ligand was weakened by the LMCT effect between the Al-O clusters and the  $\text{NH}_2\text{-H}_2\text{BDC}$  ligand formed in the Al-MOF. On the introduction of phosphate, following the pre-concentration of available sites from the positively charged  $\text{-NH}_3^+$  and Al-OH groups on the surface of Al-MOF, the high coordination between Al-O clusters and phosphate inhibited the LMCT effect and the original architecture of the Al-MOF was destroyed, releasing the organic ligand and recovering the intrinsic fluorescence in correlation with the applied phosphate level.

### 3.6 Real sample detection by a fluorescence sensor

Based on the above studies, a phosphate digital sensor was developed and equipped with professional data acquisition software. The external and internal structure of the sensor are shown in Fig. S19. The device was equipped with a silicon photodiode S1336-18BQ (Hamamatsu, Japan) and a customized 325 nm LED as the light source. The fluorescence emission intensity was steadily acquired through the sensor and the obtained data were provided to the IDSen-800 data acquisition software (Fig. S20). The detection of phosphate in deionized water, tap water, and lake water was carried out by the standard addition method in water samples. The influence of  $\text{HCO}_3^-$  and  $\text{SO}_4^{2-}$  anions in the tap water and lake water was eliminated by using the method described above. To simulate the typical concentration of phosphate in the aqueous environment, the highest spiked concentration of phosphate was set to approximately  $67 \mu\text{mol/L}$ . The obtained results for deionized water, tap water, and lake water are shown in Table 2. The relative standard deviation (RSD) values for the tap water and lake water samples were within 15%, which is in the acceptable range, and the recovery ranged from 85.1% to 111.0%. The excellent recovery and RSD values indicated that the

**Table 2** Results for on-site detection of phosphate in water samples

Samples	Spiked ( $\mu\text{mol/L}$ )	Measured ( $\mu\text{mol/L}$ ) (mean $\pm$ standard deviation, $n = 3$ )	Recovery (%)
Deionized water	14.89	14.77 $\pm$ 0.54	99.2 $\pm$ 3.6
	24.69	23.50 $\pm$ 0.02	95.2 $\pm$ 0.1
	34.40	32.83 $\pm$ 1.04	95.4 $\pm$ 3.0
	44.01	44.45 $\pm$ 1.61	101.0 $\pm$ 3.7
	53.53	55.41 $\pm$ 0.14	103.5 $\pm$ 0.3
Tap water	18.58	16.49 $\pm$ 1.57	88.8 $\pm$ 8.4
	30.77	26.18 $\pm$ 2.04	85.1 $\pm$ 6.6
	42.81	38.75 $\pm$ 2.16	90.5 $\pm$ 5.0
	54.71	50.95 $\pm$ 2.55	93.1 $\pm$ 4.7
	66.47	61.27 $\pm$ 3.03	92.2 $\pm$ 4.6
Lake water	16.53	18.35 $\pm$ 3.07	111.0 $\pm$ 18.6
	27.4	27.39 $\pm$ 3.88	100.0 $\pm$ 14.2
	38.15	39.58 $\pm$ 5.02	103.7 $\pm$ 13.2
	48.78	50.24 $\pm$ 3.53	103.0 $\pm$ 7.2
	59.3	63.10 $\pm$ 3.49	106.4 $\pm$ 5.9

phosphate detection method is effective for water samples.

## 4 Conclusions

In summary, environmentally friendly trivalent metal Al-based MOF was successfully synthesized through the facile solvothermal method for phosphate detection in aqueous environments. It was found that the as-synthesized Al-MOF possessed thermal and water stability in a wide pH range of 4–10. The fluorescence probe was able to detect phosphate with a low detection limit of 3.25  $\mu\text{mol/L}$ , which is below the threshold of phosphate concentration that gives rise to eutrophication (over 0.2 mg/L). The detection method with three different Al-MOF concentrations was used to achieve the range of 3–350  $\mu\text{mol/L}$ , meeting the requirements for the detection of phosphate discharge in aqueous environments (0.2–10 mg P/L). Additionally, the Al-MOF exhibited good selectivity toward phosphate with respect to most anions and common metal cations, and chromatographic pretreatment column adsorption and pH adjustment of the solution can eliminate the influence of the  $\text{SO}_4^{2-}$  and  $\text{HCO}_3^-$  anions. The study of the phosphate detection mechanism demonstrated that the high affinity between phosphate pre-concentrated by available sites and Al-O in Al-MOF weakened the LMCT process, and thus recovered the intrinsic fluorescence of  $\text{NH}_2\text{-H}_2\text{BDC}$ , resulting in fluorescence enhancement and enabling the development of a turn-on detection method. Furthermore, the on-site phosphate sensor based on the Al-MOF fluorescence probe was successfully developed and applied for phosphate detection in real environmental water samples. We believe that this detection method will provide a new

insight into the synthesis of LMOFs for their further application in sensing of other inorganic ions in the aqueous environment.

**Acknowledgements** This work is supported by the National Key Research and Development Program of China (No. 2021YFC3200604), the Oceanic Interdisciplinary Program of Shanghai Jiao Tong University (No. SL2020MS014).

**Electronic Supplementary Material** Supplementary material is available in the online version of this article at <https://doi.org/10.1007/s11783-022-1594-8> and is accessible for authorized users.

## References

- Chandra Rao P, Mandal S (2018). Europium-based metal-organic framework as a dual luminescence sensor for the selective detection of the phosphate anion and  $\text{Fe}^{3+}$  ion in aqueous media. Inorganic Chemistry, 57(19): 11855–11858
- Chen B, Ockwig N W, Millward A R, Contreras D S, Yaghi O M (2005). High  $\text{H}_2$  adsorption in a microporous metal-organic framework with open metal sites. Angewandte Chemie (International ed. in English), 44(30): 4745–4749
- Chen B B, Sheng Li R, Li Liu M, Yan Zou H, Liu H, Huang C Z (2018). Highly selective detection of phosphate ion based on a single-layered graphene quantum dots- $\text{Al}^{3+}$  strategy. Talanta, 178: 172–177
- Chen W, Westerhoff P, Leenheer J A, Booksh K (2003). Fluorescence excitation-emission matrix regional integration to quantify spectra for dissolved organic matter. Environmental Science & Technology, 37(24): 5701–5710
- Cheng Y, Zhang H, Yang B, Wu J, Wang Y, Ding B, Huo J, Li Y (2018). Highly efficient fluorescence sensing of phosphate by dual-emissive lanthanide MOFs. Dalton Trans, 47(35): 12273–12283
- Colina M, Gardiner P H E (1999). Simultaneous determination of total nitrogen, phosphorus and sulphur by means of microwave digestion and ion chromatography. Journal of Chromatography. A, 847(1–2): 285–290
- Dai C, Yang C X, Yan X P (2015). Ratiometric fluorescent detection of phosphate in aqueous solution based on near infrared fluorescent silver nanoclusters/metal-organic shell composite. Analytical Chemistry, 87(22): 11455–11459
- Das A, Biswas S (2017). A multi-responsive carbazole-functionalized  $\text{Zr}(\text{IV})$ -based metal-organic framework for selective sensing of  $\text{Fe}^{(\text{III})}$ , cyanide and *p*-nitrophenol. Sensors and Actuators. B, Chemical, 250: 121–131
- Das A, Das S, Trivedi V, Biswas S (2019). A dual functional MOF-based fluorescent sensor for intracellular phosphate and extracellular 4-nitrobenzaldehyde. Dalton Trans, 48(4): 1332–1343
- Fan C, Lv X, Tian M, Yu Q, Mao Y, Qiu W, Wang H, Liu G (2020). A terbium(III)-functionalized zinc(II)-organic framework for fluorometric determination of phosphate. Mikrochimica Acta, 187(1): 84
- Férey G (2008). Hybrid porous solids: Past, present, future. Chemical Society Reviews, 37(1): 191–214
- Gao N, Huang J, Wang L Y, Feng J Y, Huang P C, Wu F Y (2018).

- Ratiometric fluorescence detection of phosphate in human serum with a metal-organic frameworks-based nanocomposite and its immobilized agarose hydrogels. *Applied Surface Science*, 459: 686–692
- He J, Wang J, Chen Y, Zhang J, Duan D, Wang Y, Yan Z (2014). A dye-sensitized Pt@UiO-66(Zr) metal-organic framework for visible-light photocatalytic hydrogen production. *Chemical Communications* (Cambridge, England), 50(53): 7063–706624848342
- Horcajada P, Gref R, Baati T, Allan P K, Maurin G, Couvreur P, Férey G, Morris R E, Serre C (2012). Metal-organic frameworks in biomedicine. *Chemical Reviews*, 112(2): 1232–1268
- Kröckel L, Lehmann H, Wieduwilt T, Schmidt M A (2014). Fluorescence detection for phosphate monitoring using reverse injection analysis. *Talanta*, 125: 107–113
- Li C M, Li Y F, Wang J, Huang C Z (2010). Optical investigations on ATP-induced aggregation of positive-charged gold nanoparticles. *Talanta*, 81(4–5): 1339–1345
- Li Z P, Huang Z W, Xie N, Gao X N, Fang Y T, Zhang Z G (2018). Preparation of Al<sub>2</sub>O<sub>3</sub>-coated expanded graphite with enhanced hydrophilicity and oxidation resistance. *Ceramics International*, 44(14): 16256–16264
- Liu R T, Chi L N, Wang X Z, Wang Y, Sui Y M, Xie T T, Arandian H (2019). Effective and selective adsorption of phosphate from aqueous solution via trivalent-metals-based amino-MIL-101 MOFs. *Chemical Engineering Journal*, 357: 159–168
- Lu Z Z, Zhang R, Li Y Z, Guo Z J, Zheng H G (2011). Solvatochromic behavior of a nanotubular metal-organic framework for sensing small molecules. *Journal of the American Chemical Society*, 133(12): 4172–4174
- Ma L, Abney C, Lin W (2009). Enantioselective catalysis with homochiral metal-organic frameworks. *Chemical Society Reviews*, 38(5): 1248–1256
- Orellana-Tavra C, Marshall R J, Baxter E F, Lázaro I A, Tao A, Cheetham A K, Forgan R S, Fairén-Jiménez D (2016). Drug delivery and controlled release from biocompatible metal-organic frameworks using mechanical amorphization. *Journal of Materials Chemistry B*, 4(47): 7697–7707
- Saini A K, Srivastava M, Sharma V, Mishra V, Mobin S M (2016). A highly selective, sensitive and reversible fluorescence chemosensor for Zn<sup>2+</sup> and its cell viability. *Dalton Trans*, 45(9): 3927–3935
- Serra-Crespo P, Ramos-Fernandez E V, Gascon J, Kapteijn F (2011). Synthesis and Characterization of an amino functionalized MIL-101(Al): Separation and catalytic properties. *Chemistry of Materials*, 23(10): 2565–2572
- Shi B B, Zhang Y M, Wei T B, Lin Q, Yao H, Zhang P, You X M (2014). A fluorescent and colorimetric chemosensor for dihydrogen phosphate ions based on 2-pyridine-1H-imidazo[4,5-b]phenazine-zinc ensemble. *Sensors and Actuators B, Chemical*, 190: 555–561
- Song Y, Li Y, Liu Y, Su X, Ma Q (2015). Highly sensitive and selective detection of phosphate using novel highly photoluminescent water-soluble Mn-doped ZnTe/ZnSe quantum dots. *Talanta*, 144: 680–685
- Sun Z J, Jiang J Z, Li Y F (2015). A sensitive and selective sensor for biothiols based on the turn-on fluorescence of the Fe-MIL-88 metal-organic frameworks-hydrogen peroxide system. *The Analyst*, 140(24): 8201–8208
- Wang B, Yang Q, Guo C, Sun Y, Xie L H, Li J R (2017). Stable Zr(IV)-based metal-organic frameworks with predesigned functionalized ligands for highly selective detection of Fe(III) ions in water. *ACS Applied Materials & Interfaces*, 9(11): 10286–10295
- Wang R, Zhang Q, Zhang Y, Shi H, Nguyen K T, Zhou X (2019). Unconventional split aptamers cleaved at functionally essential sites preserve biorecognition capability. *Analytical Chemistry*, 91(24): 15811–15817
- Xie L H, Liu X M, He T, Li J R (2018). Metal-organic frameworks for the capture of trace aromatic volatile organic compounds. *Chem*, 4(8): 1911–1927
- Xu H, Cao C S, Zhao B (2015). A water-stable lanthanide-organic framework as a recyclable luminescent probe for detecting pollutant phosphorus anions. *Chemical Communications* (Cambridge, England), 51(51): 10280–1028325940110
- Xu M M, Kong X J, He T, Wu X Q, Xie L H, Li J R (2018). A stable Zr(IV)-based metal-organic framework constructed from C=C bridged Di-isophthalate ligand for sensitive detection of Cr<sub>2</sub>O<sub>7</sub><sup>2-</sup> in water. *Inorganic Chemistry*, 57(22): 14260–14268
- Yang C X, Ren H B, Yan X P (2013). Fluorescent metal-organic framework MIL-53(Al) for highly selective and sensitive detection of Fe<sup>3+</sup> in aqueous solution. *Analytical Chemistry*, 85(15): 7441–7446
- Yang J, Dai Y, Zhu X Y, Wang Z, Li Y S, Zhuang Q X, Shi J L, Gu J L (2015). Metal-organic frameworks with inherent recognition sites for selective phosphate sensing through their coordination-induced fluorescence enhancement effect. *Journal of Materials Chemistry A, Materials for Energy and Sustainability*, 3(14): 7445–7452
- Zhang Y, Sheng S, Mao S, Wu X, Li Z, Tao W, Jenkinson I R (2019). Highly sensitive and selective fluorescent detection of phosphate in water environment by a functionalized coordination polymer. *Water Research*, 163: 114883
- Zhang Z, Zhao Y, Gong Q, Li Z, Li J (2013). MOFs for CO<sub>2</sub> capture and separation from flue gas mixtures: The effect of multifunctional sites on their adsorption capacity and selectivity. *Chemical communications* (Cambridge, England), 49(7): 653–66123150882
- Zhao D, Wan X Y, Song H J, Hao L Y, Su Y Y, Lv Y (2014). Metal-organic frameworks (MOFs) combined with ZnO quantum dots as a fluorescent sensing platform for phosphate. *Sensors and Actuators B, Chemical*, 197: 50–57
- Zhu L, Zhou X H, Shi H C (2014a). A potentiometric cobalt-based phosphate sensor based on screen-printing technology. *Frontiers of Environmental Science & Engineering*, 8(6): 945–951
- Zhu X, Gu J, Wang Y, Li B, Li Y, Zhao W, Shi J (2014b). Inherent anchorages in UiO-66 nanoparticles for efficient capture of alendronate and its mediated release. *Chemical Communications* (Cambridge, England), 50(63): 8779–878224967656